We are IntechOpen, the world's leading publisher of Open Access books
Built by scientists, for scientists

6,900
Open access books available

185,000
International authors and editors

200M
Downloads

154
Countries delivered to

Our authors are among the

TOP 1%
most cited scientists

12.2%
Contributors from top 500 universities

BOOK CITATION INDEX
CLARIVATE ANALYTICS
INDEXED

WEB OF SCIENCE™

Selection of our books indexed in the Book Citation Index
in Web of Science™ Core Collection (BKCI)

Interested in publishing with us?
Contact book.department@intechopen.com

Numbers displayed above are based on latest data collected.
For more information visit www.intechopen.com

5

Local, Fine Co-Registration of SAR Interferometry Using the Number of Singular Points for the Evaluation

Ryo Natsuaki and Akira Hirose

Department of Electrical Engineering and Information Systems, The University of Tokyo

Japan

1. Introduction

Synthetic aperture radar (SAR) has great advantage of being able to observe large area accurately in any weather. It can measure various properties of the earth Boerner (2003), e.g., the topography, the vegetation Hajinsek et al. (2009), and the landscape changes caused by earthquakes or volcanoes Gabriel et al. (1989). One of the common usages of SAR is Interferometric synthetic aperture radar (InSAR), which can measure the landscape with an interferogram of SAR images. The SAR interferogram is made from two complex-valued maps obtained by observing identical place, named "master" and "slave." The phase information of the interferogram corresponds to the ground topography. To generate digital elevation model (DEM) from interferogram, phase unwrapping process is required. However, an unwrapping process is disturbed seriously by singular points (SPs), the rotational points existing in the phase map.

Most of the SPs hinder us from creating accurate DEM Ghiglia & Pritt (1998). Many researchers have tried to solve this problem by proposing novel methods concerning branch-cut techniques Costantini (1998), least squares Pritt & Shipman (1994), and singularity spreading technique Yamaki & Hirose (2007). These major methods have numerous efficient improvements e.g., Fornaro et al. (1996) Reigber & Moreia (1997) Suksmono & Hirose (2006). Various SP elimination filters have also developed and applied to the interferogram. For example, Lee filter Lee et al. (1998), Goldstein filter Goldstein & Werner (1998), Bayesian filter Ferraiuolo & Poggi (2004), and Markov random field modeled filter Suksmono & Hirose (2002) Yamaki & Hirose (2009) are the popular.

There are three origins in the SP generation. One is the low SNR caused by low scattering reflectance. Another one is the sharp cliff and layover. The landscape can be so rough that the aliasing occurs. The last one is the local distortion in the co-registration of the master and the slave. That is, the reflection, scattering and fore-shortening can be different in the two observations with slightly different sight angle, resulting in local phase distortion in the interferogram. Filtering and unwrapping methods can solve first two origins. On the other hand, the last origin, the local distortion, has been generally ignored.

Without the distortion, no SP is expected through an appropriate co-registration of non-aliasing master and slave maps. Usually the co-registration is realized by maximizing the amplitude cross-correlation of the maps in macro scale, while by maximizing the complex-amplitude correlation in micro scale. The correlations require an averaging process over a certain area for sufficient reduction of included noise. However, a wide-area averaging degrades the locality in the matching required to eliminate the distortion. This trade-off brings a limitation in the co-registration performance. In short, the difference in the reflection, scattering and fore-shortening yields local distortion, and SPs are generated inevitably by the cross-correlation process.

In this chapter, we firstly introduce the basis of InSAR and its SP problem. Secondly, we introduce a local and fine co-registration method which employs the number of SPs as evaluation criterion (SPEC method Natsuaki & Hirose (2011)). Finally, we demonstrate the effectiveness of the improvement by comparing the DEMs generated from interferograms which co-registered with and without the SPEC method. For experiment, we use the data of Mt. Fuji observed by JERS-1 which was launched by JAXA (Japan Aerospace Exploration Agency). Mt. Fuji has an ordinary single volcanic cone shape.
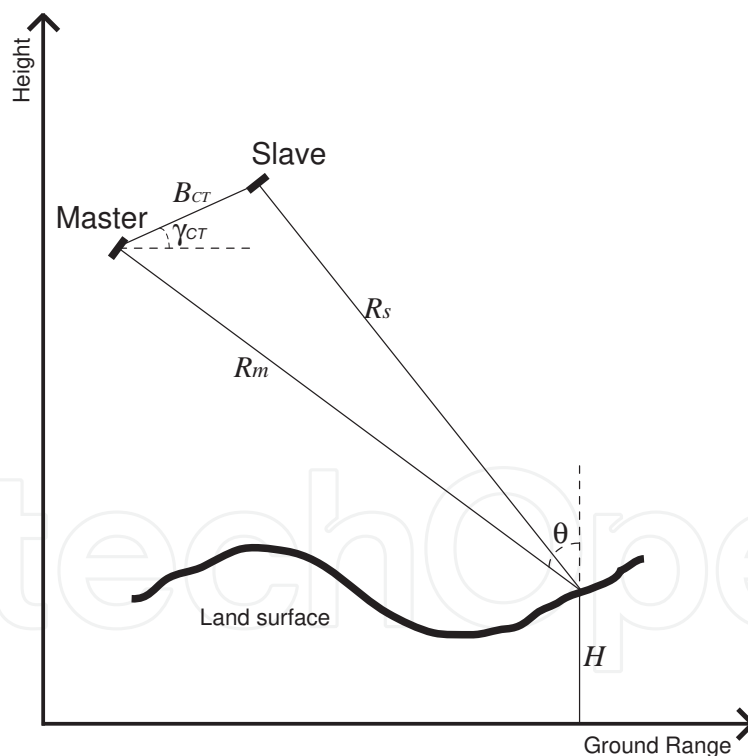
2. InSAR and SP problem

Fig. 1. Schematic diagram of InSAR

Figure 1 shows the observation system of InSAR. We define wave length as λ, elevation angle as θ, distances from ground to the master and the slave satellite as R_m and R_s, distance between the master and the slave as B_{CT}, relative angle of the master and the slave as γ_{CT}.

The phase value Φ of the interferogram corresponds to R_m and R_s as

$$\frac{\lambda \Phi}{2\pi} = 2\left(R_m - R_s\right) \tag{1}$$

Geometrically, $R_m - R_s$ corresponds to B_{CT} and γ_{CT} as

$$\left(R_m - R_s\right) = B_{CT}\sin\left(\theta - \gamma_{CT}\right) \tag{2}$$

From (1) and (2), the relationship between Φ and θ is expressed as

$$\frac{\lambda \Phi}{2\pi} = 2B_{CT}\sin\left(\theta - \gamma_{CT}\right) \tag{3}$$

If there is a height increment between the neighbor pixels, the increment of Φ is

$$\frac{\Delta \Phi}{\Delta \theta} = \frac{4\pi B_{CT}\cos(\theta - \gamma_{CT})}{\lambda} \tag{4}$$

and the increment of H is

$$\frac{\Delta H}{\Delta \theta} = R_m\sin(\theta) \tag{5}$$

From (4) and (5), the relationship between the interferogram phase increment $\Delta\Phi$ and the height increment of the observation point ΔH can be expressed as

$$\Delta H = \frac{\lambda R_m\sin(\theta)}{4\pi B_{CT}\cos(\theta - \gamma_{CT})}\Delta\Phi \tag{6}$$

which indicates that the phase gradient of 2π corresponds to the height gradient of $\frac{\lambda R_m\sin(\theta)}{2B_{CT}\cos(\theta - \gamma_{CT})}$.

In order to analyze the ground topography, we have to unwrap, line integrate, the phase information. As the ground topography is the conservative field, its contour integral should be zero.

$$\oint_c \Delta\Phi ds' = 0 \tag{7}$$

However, there are many non-zero rotational points, namely singular points (SPs), in the interferogram. As shown in Fig.2, if there is a rotational point in the interferogram, phase unwrapping will fail. We assume that there are three origins of the SP emergence.

1. Low SNR caused by low scattering reflectance
2. Sharp cliff and layover
3. Local distortion in the co-registration of the master and the slave

Origin (i) is generally thought as the main reason of SPs which should be erased. SPs generated by origin (ii) should remain. The third reason (iii) has been conventionally ignored. A pixel in the master representing a small local area should completely correspond to a pixel in the slave that represents the same area. However, we assume that the slight difference of the radar incidence direction between the master and the slave distorts this correspondence
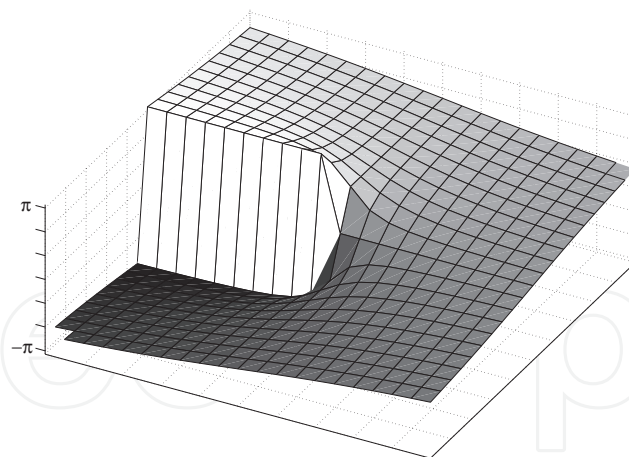
Fig. 2. Failure of unwrapping due to the existence of the SP.

in sub-pixel order, and that interferograms show these local distortions as massive SPs. In the next section, we introduce the local-o-registration method to solve the local distortion.

3. Singular points as evaluation criterion

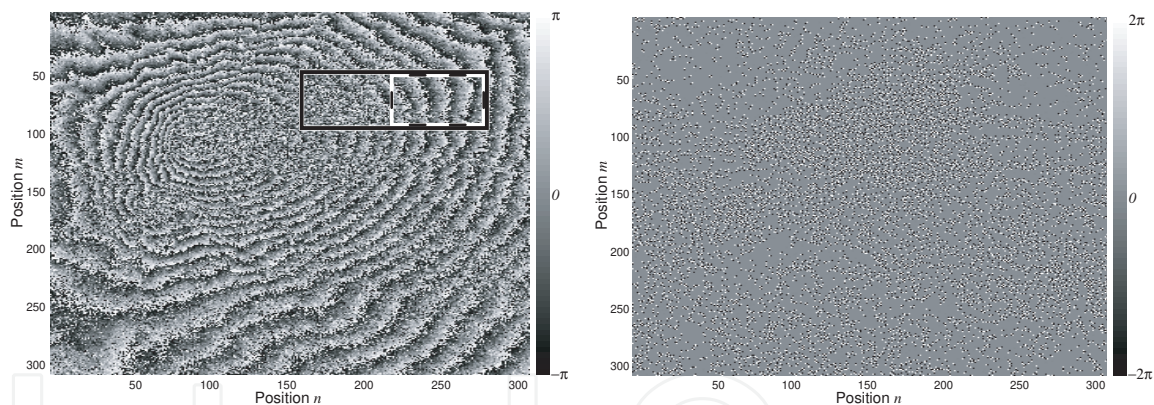### 3.1 Typical co-registration technique and the changes of SP distributions with subpixel shifts

Fig. 3. (a)Interferogram of Mt. Fuji (black square corresponds to Fig.8.) and (b)its SP plot made by the typical method (# SPs = 11,518).

To create an interferogram with master and slave, we have to co-register them in advance as they observe the same place from slightly different angle. The typical co-registration process is explained as follows Tobita et al. (1999). First, we affine-transform the slave map adaptively to maximize the cross correlation between the master and slave amplitude maps in a macro scale, e.g., 64×64 pixels. Next, we maximize the complex-valued cross correlation locally in 1/32 subpixels with interpolation, e.g., 8×8 pixels. Figure 3(a) shows the interferogram of Mt. Fuji created by this method, and Fig.3(b) gives its SP plot. This interferogram has 304×304 pixels and contains 11,518 SPs. In Fig.3(a), the phase value is shown in gray scale, in which a white dot stands for π as the phase value and a black dot means $-\pi$. In all figures in this article, the up-down direction is the azimuth and the left-right direction is the range. In Fig.3(b), a white dot indicates a clockwise SP, while a black dot shows a counterclockwise one.
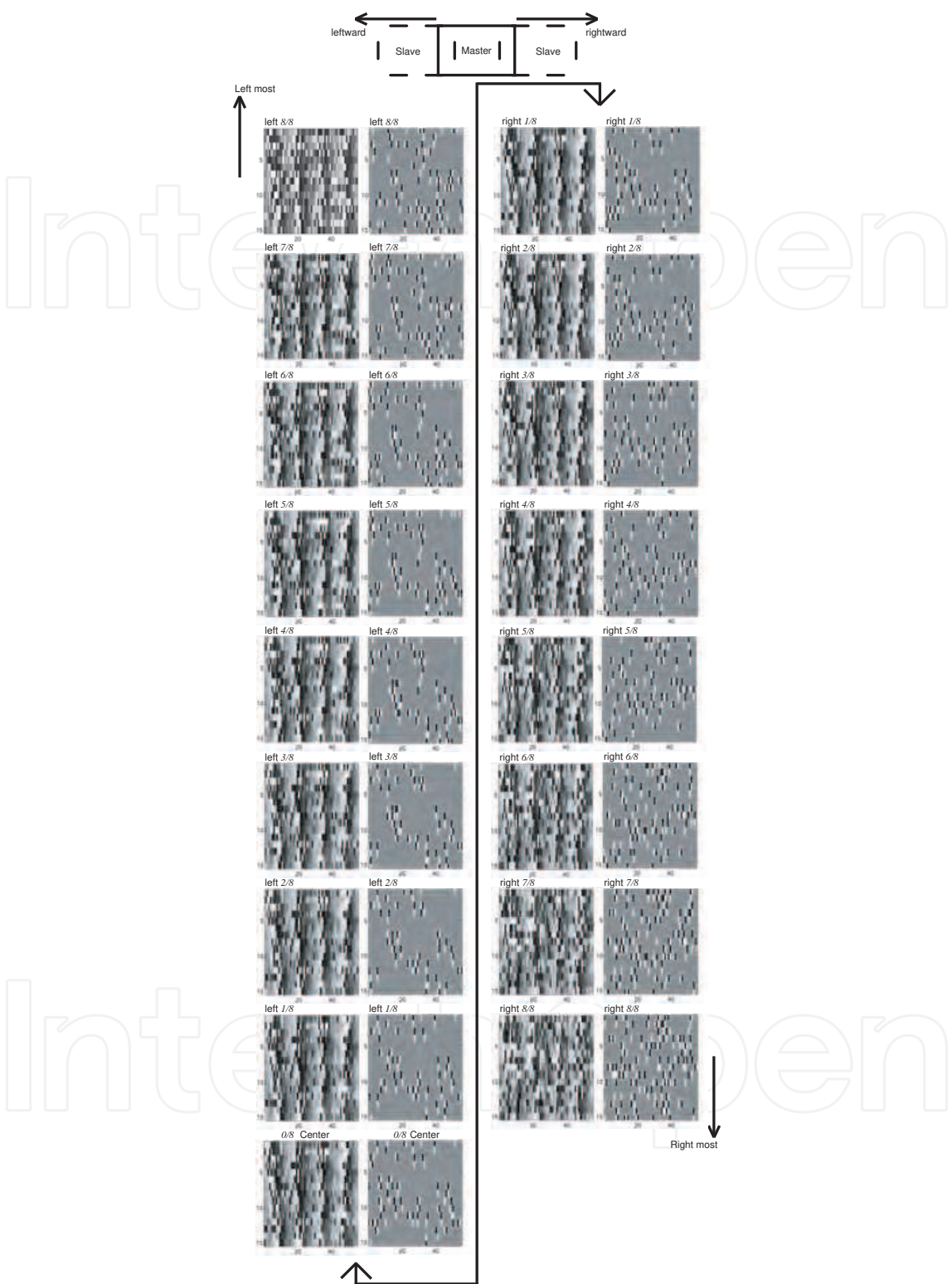
Fig. 4. Interferograms and SP plots obtained by moving the slave map from the position of maximum cross correlation leftward or rightward by integral multiple of 1/8 subpixels for the area of the right half of the black square in Fig.3(a).

Figure 4 represents how the interferogram and its SP plot change when the slave shifts leftward or rightward by integral multiple of 1/8 pixel from the maximum cross-correlation position for the right half area in the black square in Fig.3(a). It is obvious that many SPs move, emerge, or disappear, but the fringes in the interferogram show only small changes.

The emergence and the disappearance occur rather locally than the scale of correlation calculation. This fact suggests that we need a more local, and consequently nonlinear, co-registration process in addition to the conventional one. The changes in the fringes is not so large, which means that the rough landscape is not changed by this additional process, but the local precise co-registration is expected to improve the local landscape since, basically, no SPs are expected in non-distorted interferogram.

The aim of our proposal is to improve the accuracy of DEM by removing the local distortion. In this removal process, we pay attention to the number of SPs as explained in the following section. Based on this idea which came from the result of the above preliminary experiment, we introduce our new method below.

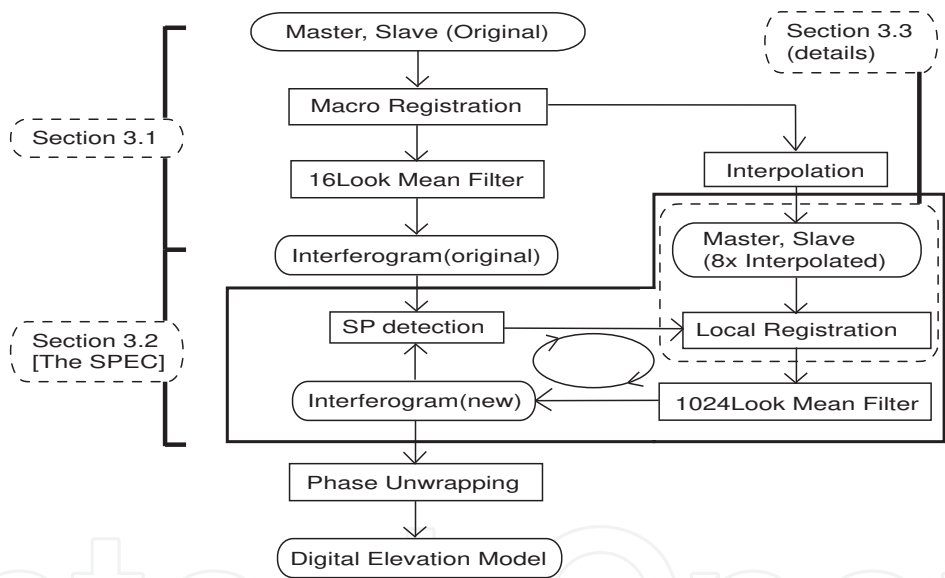### 3.2 Proposal of the SPEC method

Fig. 5. Flowchart of the whole co-registration process including the SPEC method.

Figure 5 is the flowchart of the whole co-registration process including our SPEC method. First, we co-register master M and slave S by the conventional method as explained in Section 3.1. Then we make an interferogram I from master M and slave S with 16-look mean-filtering as

$$I(m,n) = \frac{1}{16} \sum_{q=1}^{8} \sum_{p=1}^{2} M(p,q;m,n) S^*(p,q;m,n). \tag{8}$$

Fig. 6(a) explains the process. We regard the 8×2 pixels in the master and the slave as single blocks, $\mathbf{M}(m,n)$ and $\mathbf{S}(m,n)$, respectively, each of which pair yields one pixel in 16-look interferogram shown in Fig. 6(a). $M(p,q;m,n)$ represents the p-th top and q-th left pixel in the block $\mathbf{M}(m,n)$. The 16-look mean-filtering works to decrease the noise by averaging
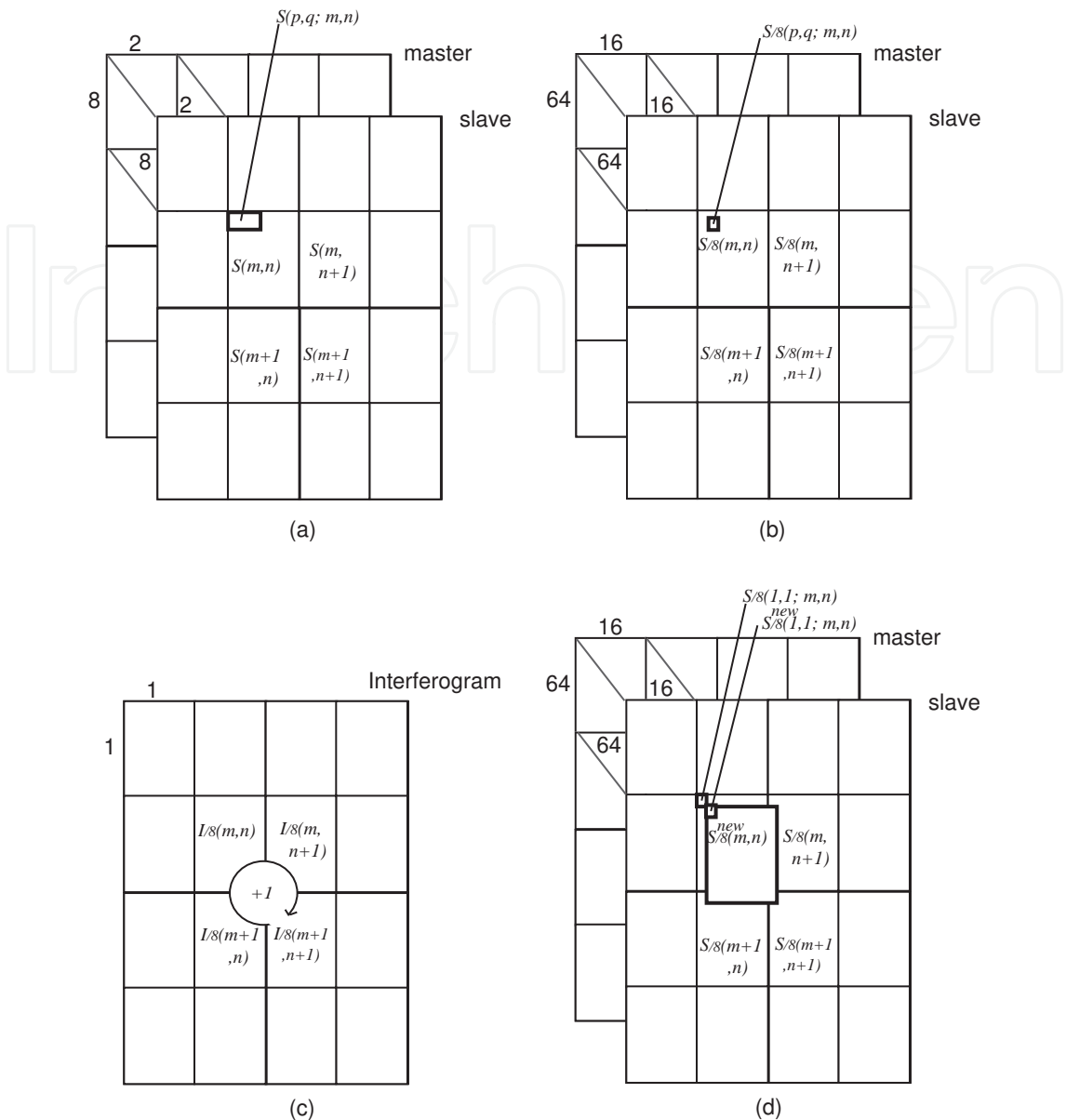
Fig. 6. Relationship between the blocks and the interferogram pixels: (a)Blocks for making regular 16-look mean-filtered interferogram in 1 pixel coordinate system, (b)blocks equal to (a) in 1/8-pixel coordinate system, (c)a SP in the interferogram made in 1/8-pixel coordinate system, and (d)local movement of the interpolated slave to delete the SP.

16 (=8×2) interferogram pixels. That is, to make an interferogram, in this paper, 8 times azimuth compression and 2 times range compression are required (i.e., to make a 304×304 pixels interferogram, 2432×608 pixels master and slave are required). Next, we find SPs in it and co-register interpolated master with interpolated slave locally and nonlinearly as follows.

3.3 Details of the local and nonlinear co-registration based on the number of SPs

Figures 6 and 7 are schematic diagrams of our local and nonlinear co-registration based on the number of SPs. We call the 8-times interpolated master and slave maps as "1/8-pixel

Fig. 7. The process of moving the slave: (a)Move $\mathbf{S}_{/8}(m,n)$ by 1/8 pixel as $S_{/8}^{\mathrm{new}}(p,q;m,n) \leftarrow S_{/8}(p-1,q-1;m,n)$ in order to erase the SP made by the 4 blocks, (b)replace back $S_{/8}^{\mathrm{new}}(p,q;m,n)$ and do the same process to $\mathbf{S}_{/8}(m,n+1)$, (c)move $S_{/8}^{\mathrm{new}}(p,q;m,n)$ by 1/8 pixel to a different direction, and (d)move $S_{/8}^{\mathrm{new}}(p,q;m,n)$ by 2/8 pixels.

coordinate-system" maps, and the original ones as "1-pixel coordinate-system" maps. Table 1 lists the definitions used here, in which $I_{/8}(m,n)$ denotes the pixel value of interferogram in the 1/8-pixel coordinate system, and $I(m,n)$ denotes the value in the 1-pixel coordinate system simply. Coordinate (m,n) stands for global position in the (16-look) mean-filtered interferogram, while (p,q) represents the local position in the 1/8-pixel coordinate system.

To get $I_{/8}(m,n)$, on the other hand, we need $(8 \times 8) \times (2 \times 8) = 1024$ subpixels. Hence we regard these 1024 pixels as single blocks, $\mathbf{M}_{/8}(m,n)$ and $\mathbf{S}_{/8}(m,n)$, respectively.

Map	Status	Notation	Unit
interferogram	16-look mean-filtered	$I(m,n)$	mean-filtered pixel
interferogram	1024-look mean-filtered in 8-times interpolation	$I_{/8}(m,n)$	mean-filtered pixel
original master, slave	single look	$M(p,q;m,n)$ $S(p,q;m,n)$	pixel
8×2 pixel block in master, slave	single look	$\mathbf{M}(m,n)$ $\mathbf{S}(m,n)$	block
8-times interpolated master, slave	8-times interpolated	$M_{/8}(p,q;m,n)$ $S_{/8}(p,q;m,n)$	subpixel
8-times interpolated block	8-times interpolated	$\mathbf{M}_{/8}(m,n)$ $\mathbf{S}_{/8}(m,n)$	block

Table 1. Map status and notation

We first make an 1/8-pixel coordinate-system interferogram locally. The pixel value $I_{/8}(m,n)$, which corresponds to a pixel of a 16-look mean-filtered interferogram $I(m,n)$, is calculated as

$$I_{/8}(m,n) = \frac{1}{1024} \sum_{q=1}^{64} \sum_{p=1}^{16} M_{/8}(p,q;m,n)S_{/8}^*(p,q;m,n) \qquad (9)$$

where $M_{/8}(p,q;m,n)$ represents the p-th top and q-th left pixel in the block $\mathbf{M}_{/8}(m,n)$, while $S_{/8}(p,q;m,n)$ represents the p-th and q-th pixel in $\mathbf{S}_{/8}(m,n)$ in the same manner. For example, if there is a SP at $I_{/8}(m,n), I_{/8}(m+1,n), I_{/8}(m,n+1), I_{/8}(m+1,n+1)$ in the interferogram, as shown in Fig.6(c), we find non-zero rotation as

$$\left|\left(\theta_{/8}(m+1,n) - \theta_{/8}(m,n)\right) + \left(\theta_{/8}(m,n) - \theta_{/8}(m,n+1)\right)+\right.$$

$$\left.\left(\theta_{/8}(m+1,n+1) - \theta_{/8}(m+1,n)\right) + \left(\theta_{/8}(m+1,n+1) - \theta_{/8}(m,n+1)\right)\right| \geq 2\pi \qquad (10)$$

where

$$\theta_{/8}(m,n) \equiv \arg(I_{/8}(m,n)). \qquad (11)$$

Simultaneously, in this square $I_{/8}(m,n)$—$I_{/8}(m+1,n+1)$, there is local distortion in the master and / or the slave. Then we therefore move one or some of the blocks among the four $\mathbf{S}_{/8}(m,n)$—$\mathbf{S}_{/8}(m+1,n+1)$ blocks to modify the interferogram. For example, we move $\mathbf{S}_{/8}(m,n)$ locally in such a manner that $S_{/8}^{\text{new}}(p,q;m,n) \leftarrow S_{/8}(p+1,q+1;m,n)$ to try to erase the SP as shown in Fig.6(d). That is, in this particular case, we shift the pixels as

$$\begin{pmatrix} S_{/8}^{\text{new}}(1,1;m,n) & S_{/8}^{\text{new}}(1,2;m,n) & \dots & S_{/8}^{\text{new}}(1,16;m,n) \\ S_{/8}^{\text{new}}(2,1;m,n) & S_{/8}^{\text{new}}(2,2;m,n) & \dots & S_{/8}^{\text{new}}(2,16;m,n) \\ \vdots & \vdots & \ddots & \vdots \\ S_{/8}^{\text{new}}(64,1;m,n) & S_{/8}^{\text{new}}(64,2;m,n) & \dots & S_{/8}^{\text{new}}(64,16;m,n) \end{pmatrix}$$

$$\longleftarrow \begin{pmatrix} S_{/8}(1,1;m,n) & S_{/8}(1,1;m,n) & \dots & S_{/8}(1,16;m,n) \\ S_{/8}(2,1;m,n) & S_{/8}(1,1;m,n) & \dots & S_{/8}(1,15;m,n) \\ \vdots & \vdots & \ddots & \vdots \\ S_{/8}(64,1;m,n) & S_{/8}(63,1;m,n) & \dots & S_{/8}(63,15;m,n) \end{pmatrix} \quad (12)$$

There are nesting stages in our method. First, we move the slave by 1/8 pixel and replace $\mathbf{S}_{/8}(m,n)$ as $S_{/8}^{\mathrm{new}}(p,q;m,n) \leftarrow S_{/8}(p-1,q-1;m,n)$ as shown in Fig.7(a). Then we check whether the SP disappears with this operation or not. If it does not, we move $\mathbf{S}_{/8}(m,n+1)$, $\mathbf{S}_{/8}(m+1,n)$, and $\mathbf{S}_{/8}(m+1,n+1)$ in the slave in turn, in the same direction (Fig.7(b)). If it is impossible to erase the SP with the above up-leftward movements, we employ other seven directions (Fig.7(c)). Then for the remaining SPs, we try 2/8 shifts in the same way (Fig.7(d)). If the SP cannot be removed with up to 8/8(=1) shifts, we abandon the elimination of the SP there, and try to erase the next one in the interferogram.

We apply the above process to all of the SPs in the interferogram iteratively. If we find that there is no erasable SP any more, we apply a similar shifting process for 4 (=2 × 2) big blocks. For example, we shift $\mathbf{S}_{/8}(m,n)$, $\mathbf{S}_{/8}(m,n+1)$, $\mathbf{S}_{/8}(m+1,n)$, and $\mathbf{S}_{/8}(m+1,n+1)$ simultaneously as a single large block.

$$\begin{pmatrix} S_{/8}^{\mathrm{new}}(1,1;m,n) & S_{/8}^{\mathrm{new}}(1,2;m,n) & \dots & S_{/8}^{\mathrm{new}}(1,16;m,n+1) \\ S_{/8}^{\mathrm{new}}(2,1;m,n) & S_{/8}^{\mathrm{new}}(2,2;m,n) & \dots & S_{/8}^{\mathrm{new}}(2,16;m,n+1) \\ \vdots & \vdots & \ddots & \vdots \\ S_{/8}^{\mathrm{new}}(64,1;m+1,n) & S_{/8}^{\mathrm{new}}(64,2;m+1,n) & \dots & S_{/8}^{\mathrm{new}}(64,16;m+1,n+1) \end{pmatrix}$$

$$\longleftarrow \begin{pmatrix} S_{/8}(1,1;m,n) & S_{/8}(1,1;m,n) & \dots & S_{/8}(1,16;m,n+1) \\ S_{/8}(2,1;m,n) & S_{/8}(1,1;m,n) & \dots & S_{/8}(1,15;m,n+1) \\ \vdots & \vdots & \ddots & \vdots \\ S_{/8}(64,1;m+1,n) & S_{/8}(63,1;m+1,n) & \dots & S_{/8}(63,15;m+1,n+1) \end{pmatrix} \quad (13)$$

We can also apply a 9 (=3 × 3) bigger block movement afterward, if needed.

4. Experimental results

Figure 8 presents the changes of the phase map and corresponding SP distributions when we apply the SPEC method. The shown area is the black-squared part in Fig.3(a). As shown in Figs.8(a) and (b), there were 1,014 SPs in the original interferogram. The first iteration in our proposed method erased more than 60 percent of them, resulting in 396 SPs (Figs.8(c) and (d)). In the second iteration, 324 points left (Figs.8(e) and (f)). For the present data, with 1-block movement, no SP was erased anymore. With the additional 4-block move, our proposed method decreased the SP number to 184 (Figs.8(g) and (h)). With the 9-block move, our method decreased the SP number to 171 (Figs.8(i) and (j)), where our method finally erased about 83% of the SPs in the original interferogram. Figures 9(a) and 9(b) show the resulting interferogram and its SP plot for the data in Fig.3(a). The number of the SPs decreased from 11,518 to 1,865. The decreasing ratio was about 83% again for the whole interferogram.

Figure 10 compares (a) the true height map and the results of the unwrapping by the iterative least-square (LS) techniqueSuksmono & Hirose (2006) (b) with and (c) without the SPEC
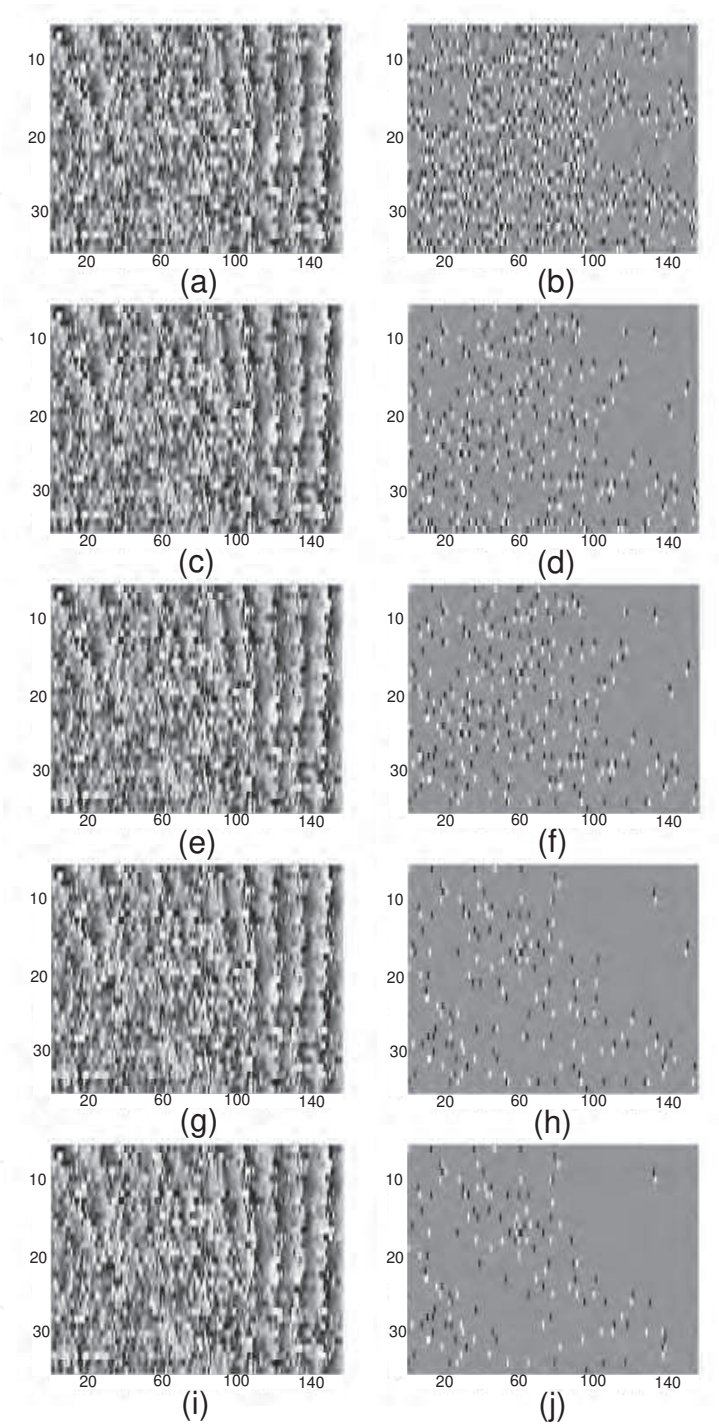
Fig. 8. Interferogram and its SP plot for the black-square area in Fig.3(a): (a)Interferogram before the local co-registration process and (b)its SP plot (1,014 SPs), (c)result of the first iteration with 1-block shifts and (d)its SP plot (396 SPs), (e)result of the second iteration with 1-block shifts and (f)its SP plot (324 SPs), (g)result of 4-block shifts in addition and (h)its SP plot (184 SPs), and (i)result of 9-block shifts in addition and (j)its SP plot (171 SPs).
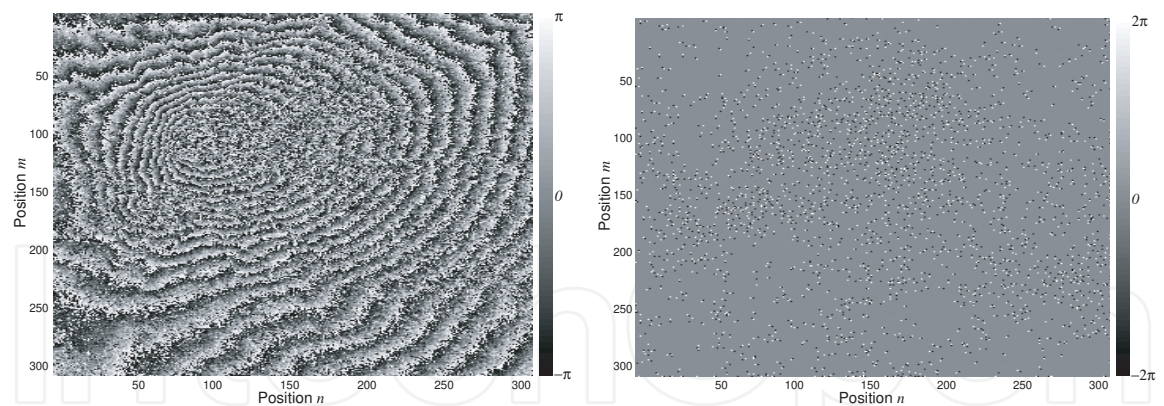
Fig. 9. (a)Interferogram made by the proposed SPEC method for the data shown in Fig.3(a) and (b)its SP plot (# SPs = 1,865).

method. We find improvement in some regions in the SPEC result in (b). For example, the dotted-square region in Fig.10(b) (zoomed in Fig. 11) shows more accurate ridges than those in Fig.10(c). It is obvious that the valleys and edges in Fig.11(b) are more distinct than those in Fig.11(c). We compared the mean signal-to-noise ratio (MSNR) ($\equiv$ squared height range / mean squared error) and the peak signal-to-noise ratio (PSNR) ($\equiv$ squared height range / peak squared error) based on the true data. The DEM with the SPEC method resulted in $MSNR = 29.5$[dB] and $PSNR = 14.5$[dB]. On the other hand, the DEM without our method resulted in $MSNR = 27.2$[dB] and $PSNR = 14.3$[dB]. The SPEC method improved the quality of the DEM both in average and at the peak.

We intend that our SPEC method compensates the local phase distortions in the interferogram. As this ability is similar to filtering (i.e., phase estimation), we calculated whether the SNR of the filtered interferogram changes if we co-register the interferogram with our proposed method. We used the iterative LS technique for unwrapping and the complex-valued Markov random field model (CMRF) filter Yamaki & Hirose (2009) for this evaluation. We compared the results for filtered interferograms of Mt. Fuji with those of non-filtered ones, which are co-registered with and without our SPEC method.

Co-registration Filtering		Without SPEC method	With SPEC method
Without filter	MSNR [dB]	27.2	29.5
	PSNR [dB]	14.3	14.5
With the CMRF filter	MSNR [dB]	35.8	34.9
	PSNR [dB]	19.2	19.7

Table 2. MSNR and PSNR of Mt. Fuji's DEMs unwrapped by the iterative LS

Table 2 shows the results of this experiment. The CMRF filter increased the SNRs of the DEMs of Mt. Fuji. Table 2 shows that the use of the SPEC method could not improve the MSNR of Mt. Fuji. The reason of this result is that the shape of the mountains and the phase ambiguity led to this result. Mt. Fuji has an ordinary single volcanic cone shape with clear fringes. Basically, phase estimation works good when the interferogram has clear fringes. As our SPEC method is an additional step of co-registration, it decreases the number of SPs and make fringes clearer
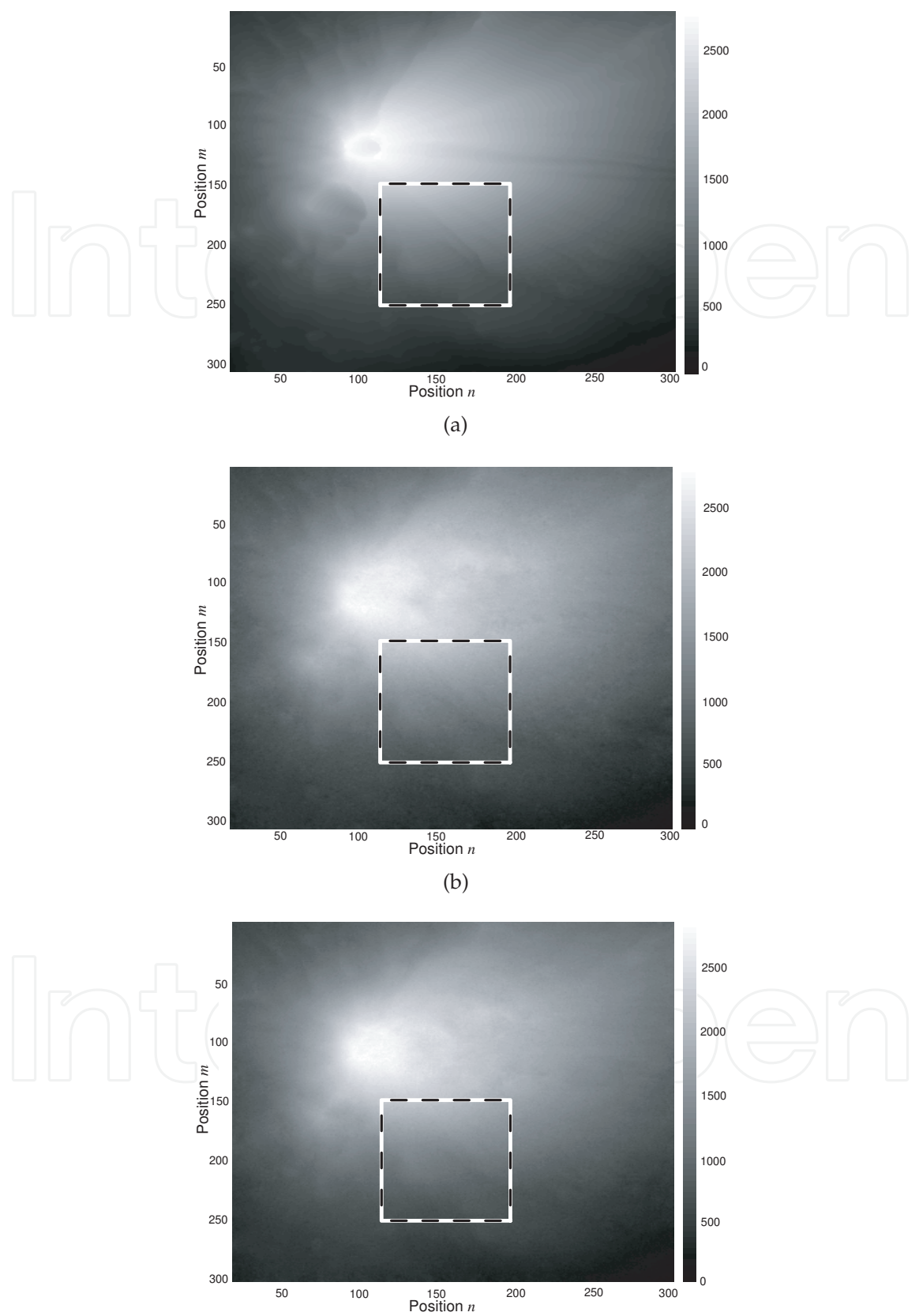
(a)

(b)

(c)

Fig. 10. (a)True height map and DEMs obtained by the iterative least square technique(b)with and (c)without the SPEC method (Mt. Fuji).
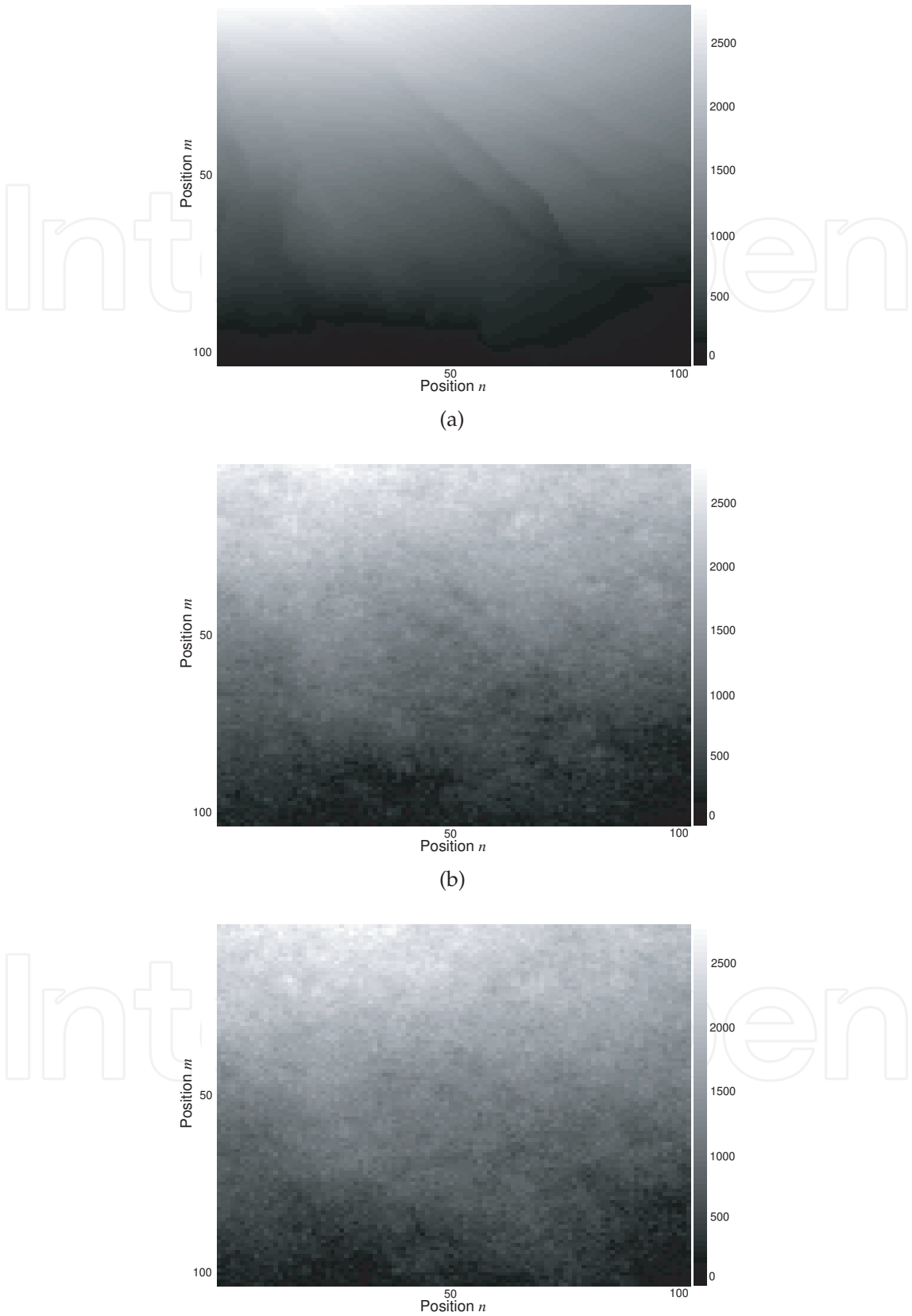
(a)

(b)

(c)

Fig. 11. Dotted square part of Fig.10. (a)True height map and DEMs obtained (b)with and (c)without the SPEC method.

before the CMRF filter works. That is why the CMRF filter could estimate the fringes of the interferogram more precisely.

5. Conclusion

We proposed a new method of co-registration, namely, the SPEC method. This method uses the number of SPs in the temporary interferogram as the evaluation criterion to co-register the master and slave maps locally and nonlinearly. By applying our method to real data, we found that the SPEC method successfully improves the quality of the DEM in many cases.At the same time, we found that the SPEC method make ambiguous fringes clearer in its appearance. Our present method uses only the number of singular points as the evaluation criterion. In the future, we have the possibility to use other information, in addition to the SP number, to improve the performance further.

6. Acknowledgment

The authors would like to thank Dr. M. Shimada of EORC/JAXA, Japan, for supplying the InSAR data and the height data for evaluation.

7. References

Boerner, W. M. (2003). "Recent advances in extra-wide-band polarimetry, interferometry and polarimetric interferometry in synthetic aperture remote sensing and its applications," *IEE Proceedings Radar, Sonar and Navigation,* Vol.150, No.3, pp.113-124, June 2003.

Costantini, M. (1998). "A Novel Phase Unwrapping Method Based on Network Programming," *IEEE Transactions on Geoscience and Remote Sensing*, vol. 36, no. 3, pp. 813-821, May 1998.

Ferraiuolo, G. & Poggi, G. (2004), "A Bayesian Filtering Technique for SAR Interferometric Phase Fields," *IEEE Transactions on Image Processing*, Vol.13, No.10, pp.1368-1378, October 2004.

Fornaro, G.; Franceschetti, G., & Lanari, G. (1996) "Interferometric SAR phase unwrapping using Green's formulation,"*IEEE Transactions on Geoscience and Remote Sensing*, vol. 34, no. 3, pp. 720-727, May 1996.

Gabriel, A. K.; Goldstein, R. M. & Zebker, H. A. (1989). "Mapping small elevation changes over large areas: Differential interferometry," Journal of Geophysical Research, vol. 94, pp. 9183-9191, July 1989.

Ghiglia, D. C. & Pritt, M. D. (1998). "Two-Dimensional Phase Unwrapping : Theory," *Algorithms, and Software. John Wiley and Sons, Inc.*, 1998.

Goldstein, R. and Werner, C. (1998). "Radar interferogram filtering for geophysical applications,"*Geophysical Research Letters*, vol. 25, no. 21, pp. 4035-4038, November 1998.

Hajnsek, I.; Jagdhuber, T.; Schon, H. & Papathanassiou, K. P. (2009). "Potential of Estimating Soil Moisture Under Vegetation Cover by PolSAR," *IEEE Transactions on Geoscience and Remote Sensing*, Vol.47, No.2, pp. 442-454, February 2009.

Lee, J. S.; Papathanassiou, K. P.; Ainsworth, T. L.; Grunes, M. R. & Reigber, A. (1998). "A new technique for noise filtering of sar interferometric phase images,"*IEEE Transactions on Geoscience and Remote Sensing*, vol. 36, pp. 1456-1464, Sept. 1998.

Natsuaki, R. & Hirose A. (2011). "SPEC Method – A fine co-registration method for SAR interferometry," *IEEE Transactions Geoscience and Remote Sensing*, Vol.49, No.1, pp. 28-37, January 2011.

Pritt, M. & Shipman, j. (1994). "Least-squares two-dimensional phase unwrapping using FFT's," *IEEE Transactions on Geoscience and Remote Sensing*, vol. 32, no. 3, pp. 706-708, May 1994.

Reigber, A. & Moreia, J. (1997). "Phase unwrapping by fusion of local and global methods," in *International Geoscience and Remote Sensing Symposium (IGARSS) 1997*, pp. 869-871, August 1997.

Suksmono, A. B. & A. Hirose, A. (2002). "Adaptive noise reduction of InSAR images based on a complex-valued MRF model and its application to phase unwrapping problem," *IEEE Transactions on Geoscience and Remote Sensing*, Vol.40, No.3, pp.699-709, March 2002.

Suksmono, A. B. and Hirose, A. (2006). "Progressive transform-based phase unwrapping utilizing a recursive structure,"*IEICE Transactions on Communications*, vol. E89-B, no. 3, pp. 929-936, Mar. 2006.

Tobita, M.; Fujiwara, S.; Murakami, M.; Nakagawa, H. & Rosen, P. A. (1999). "Accurate offset estimation between two SLC images for SAR interferometry" (in Japanese), *Journal of the Geodetic Society of Japan*, 45, 297-314, 1999.

Yamaki, R. & Hirose, A. (2007). "Singularity-Spreading Phase Unwrapping," *IEEE Transactions on Geoscience and Remote Sensing*, Vol.45, No.10, Oct. 2007.

Yamaki, R. & Hirose, A. (2009). "Singular Unit Restoration in Interferograms Based on Complex-valued Markov Random Field Model for Phase Unwrapping," *IEEE Geoscience and Remote Sensing Letters*, Vol.6, No.1, pp.18-22, January 2009.
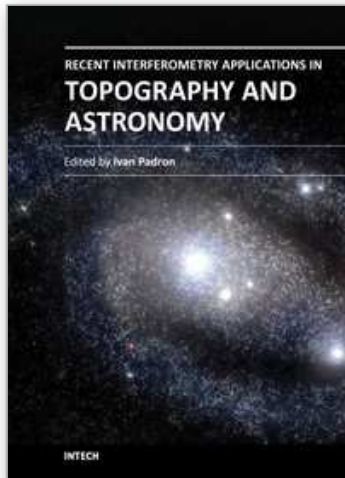
Recent Interferometry Applications in Topography and Astronomy

Edited by Dr Ivan Padron

This book provides a current overview of the theoretical and experimental aspects of some interferometry techniques applied to Topography and Astronomy. The first two chapters comprise interferometry techniques used for precise measurement of surface topography in engineering applications; while chapters three through eight are dedicated to interferometry applications related to Earth's topography. The last chapter is an application of interferometry in Astronomy, directed specifically to detection of planets outside our solar system. Each chapter offers an opportunity to expand the knowledge about interferometry techniques and encourage researchers in development of new interferometry applications.

How to reference

In order to correctly reference this scholarly work, feel free to copy and paste the following:

Ryo Natsuaki and Akira Hirose (2012). Local, Fine Co-Registration of SAR Interferometry Using the Number of Singular Points for the Evaluation, Recent Interferometry Applications in Topography and Astronomy, Dr Ivan Padron (Ed.), ISBN: 978-953-51-0404-9, InTech, Available from: http://www.intechopen.com/books/recent-interferometry-applications-in-topography-and-astronomy/local-fine-co-registration-of-sar-interferometry-using-the-number-of-singular-points-for-the-evaluat

INTECH
open science | open minds